TELKOMNIKA Indonesian Journal of Electrical Engineering
Vol.12, No.5, May 2014, pp. 3544 ~ 3554
DOI: http://dx.doi.org/10.11591/telkomnika.v12i5.3587

Acoustic Emission Source Identification Based on Pattern Recognition Method

Zhigang Feng*, Jiu Yao
School of Automation, Shenyang Aerospace University, Liaoning, 110136, P.R.China
*Corresponding author, e-mail: fzg1023@yeah.net

Abstract

A new pattern recognition method based on harmonic wavelet packet (HWPT) and hierarchy support vector machine (H-SVM) is proposed to solve the fatigue damage identification problem of helicopter component. In this approach, HWPT is used to extract the energy feature of acoustic emission (AE) signals on different frequency bands and to reduce the dimensionality of original data features. The H-SVM classifier is used to identify the AE source type. A subset of the experimental data for known AE source type is used to train the H-SVM classifier, the remaining set of data is used to test the H-SVM classifier. Also, the pressure off experiment on specimen of carbon fiber materials is investigated. The results indicate that the proposed approach can implement AE source type identification effectively, and has better performance on computational efficiency and identification accuracy than wavelet packet (WPT) feature extraction and RBF neural network classification.

Keywords: *harmonic wavelet packet, support vector machine, RBF neural network, acoustic emission, pattern recognition*

1. Introduction

Due to the fact that helicopter moving components are easy to produce fatigue damage such as cracks, which are seriously endanger the operating stability and safety of helicopter, it is necessary to monitor the initiation of cracks and to master the developing trend of the cracks. Acoustic emission (AE) is a noticeable choice of nondestructive testing method because of its extremely high sensitivity. AE has been proved to be a very sensitive method for defect recognition of composite materials which have been used in typical application areas such as aerospace, vehicle industry and infrastructure. Interest towards automatic recognition of defect types based on their AE signals has increased and many recent studies have been published [1-3]. In the AE technique, AE source type identification is used to determine the model of fatigue damage.

AE source type identification is a typical problem of pattern recognition, which includes two steps, i.e. feature extraction and pattern classification. AE signals are non-stationary signals, so the traditional techniques in the time and frequency domains are not suitable for analyzing them. The wavelet transform (WT) has been demonstrated as an alterative tool for feature extraction. The scaling operation in wavelet transform produces a series of wavelet functions with different window sizes, enabling multi-resolution analysis that is suited for representing the non-stationary signals. A major drawback of wavelet transform is its low-frequency resolution in the high frequency range. The wavelet packet transform (WPT), in comparison, further decomposes the detailed information of the signal, which has been successfully applied in the feature extraction of sensor fault and machine health diagnosis [4-6]. Of the different types of wavelets developed, the harmonic wavelet possesses compact frequency expression and has overcome the limitations of traditional wavelet including energy leakage, inflexible frequency band selection and different frequency resolutions on different levels [7-8]. So in this research, harmonic wavelet packet transform is used to extract the feature of AE sources.

Numerous pattern recognition methods have been developed within the intelligent systems. Among the methods, statistical learning method and ANN are mostly used in AE signals analysis of composite materials. ANN has been widely applied in AE signal classification problems based on learning pattern from examples or empirical data modeling in the last two

Received June 19, 2013; Revised December 12, 2013; Accepted January 3, 2014

decades [9-12]. However, as a typical machine learning classifier, the ANN method is based on the empirical risk minimization principle, which has been recognized as a method that cannot always minimize the actual risk. The traditional neural network approaches have limitations on generalization giving rise to modals that can over-fit the data. This deficiency is due to the optimization algorithms used in ANN for the selection of parameters and the statistical measures used to select the model. Meanwhile, the effectiveness of the ANN methods is closely related to the number of training samples. In most cases, it is difficult to obtain large sample sets of AE signals in composite material and the effectiveness of the ANN methods can hardly be improved.

In order to overcome the disadvantages of ANN, support vector machine (SVM) is used for classification of AE sources. SVM, based on statistical learning theory, is gaining applications in the areas of machine learning, computer vision and pattern recognition because of the high accuracy and good generalization capability. The SVM training seeks a global optimal solution and avoid over fitting, so it has the ability to deal with a large number of features. It is very suitable for pattern recognition with small samples.

In this paper, we discuss the application of harmonic wavelet packet in feature extraction and hierarchy support vector machine classification in AE source type identification, and verify the algorithm using pressure off experiment on specimen of carbon fiber materials.

2. AE Source Feature Extraction Based on Harmonic Wavelet Packet

2.1. Harmonic Wavelet

In essence, the wavelet transform characterizes the correlation or similarity between the signal to be analyzed and the mother wavelet function. Such a correlation is expressed by the wavelet coefficients associated with the wavelet transform, which can be calculated through a correlation operation between the signal $x(t)$ and the conjugate $\overline{w}(t)$ of the chosen mother wavelet $w(t)$:

$$W(t)=\int_{-\infty}^{+\infty}x(\tau)\overline{w}(\tau-t)d\tau \tag{1}$$

If the signal $x(t)$ is closely correlated with the mother wavelet $w(t)$; the wavelet coefficient $\overline{w}(t)$ will be large, indicating a good match between the mother wavelet and the signal being analyzed. As a result, the information embedded in the signal can be extracted by analyzing the wavelet coefficients with local maxima. At 1993, professor D.E.Newland [13-15] from Cambridge University proposed the harmonic wavelet which has ideal 'Box-like' characteristic in frequency domain. In this study, the harmonic wavelet is chosen as the mother wavelet, due to the simplicity of its expression in the frequency domain, and is defined by:

$$H_{m,n}(\omega)=\begin{cases}1/2\pi(n-m) & m2\pi\le\omega\le n2\pi\\ 0 & elsewhere\end{cases} \tag{2}$$

Where m and n are the scale parameters. These parameters are real but not necessarily the integers. By taking the inverse Fourier transform of $H_{m,n}(\omega)$, the time domain expression of the harmonic wavelet is obtained as:

$$h_{m,n}(t)=[\exp(in2\pi t)-\exp(im2\pi t)]/i2\pi(n-m)t \tag{3}$$

If the harmonic wavelet is translated by a step $k/(n-m)\quad k\in Z$, in which k is the translation parameter, a generalized expression that is centered at $t=k/(n-m)$ with a bandwidth of $2(n-m)\pi$ can be obtained as:

$$h_{m,n}(t-\frac{k}{n-m})=\frac{\exp[in2\pi(t-\frac{k}{n-m})]-\exp[im2\pi(t-\frac{k}{n-m})]}{i2\pi(n-m)(t-\frac{k}{n-m})} \tag{4}$$

Based on the generalized expression, the harmonic wavelet transform of a signal *x*(t) can be performed as:

$$hwt(m,n,k) = \frac{(n-m)}{N}\sum_{r=0}^{N-1} x(r)h_{m,n}(r - \frac{k}{n-m}) \quad (5)$$

Where $hwt(m,n,k)$ is the harmonic wavelet coefficient. By taking the Fourier transform of Equation (5), an equivalent expression of the harmonic wavelet transform in the frequency domain can be expressed as:

$$HWT(m,n,\omega) = X(\omega)\overline{H}_{m,n}[(n-m)\omega] \quad (6)$$

Where $X(\omega)$ is the Fourier transform of the signal *x*(*t*), and $\overline{H}_{m,n}[(n-m)\omega]$ is the conjugate of $H_{m,n}[(n-m)\omega]$, which is the Fourier transform of the harmonic wavelet at the scale (*m*, *n*). Since the harmonic wavelet has compact frequency expression, as shown in Equation (2), the harmonic wavelet transform can be readily obtained through a pair of Fourier transform and inverse Fourier transform operations.

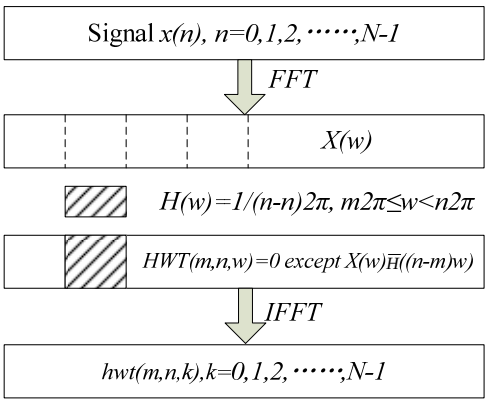

Figure 1. Algorithm for Implementing the Harmonic Wavelet Transform [8]

As shown in Figure 1, after taking the Fourier transform of a signal *x*(*t*) to obtain its frequency domain expression $X(\omega)$, the inner product $HWT(m,n,\omega)$ of $X(\omega)$ and the conjugate of the harmonic wavelet $\overline{H}_{m,n}[(n-m)\omega]$ at the scale (*m*, *n*) is calculated. Finally, the harmonic wavelet transform of the signal *x*(*t*), denoted as $hwt(m,n,k)$ is obtained by taking the inverse Fourier transform of the inner product $HWT(m,n,\omega)$.

2.2. Harmonic Wavelet Packet Algorithm

The scale parameter *m* and *n* determine the bandwidth that the harmonic wavelet covers. Similar to the Wavelet Packet Transform (WPT), the number of frequency sub-bands for the Harmonic Wavelet Packet Transform (HWPT) has to be *s* powers of 2, in which *s* corresponds to the decomposition level for WPT. Accordingly, the signal can be decomposed into 2^s frequency sub-bands with the bandwidth in Hertz for each sub-band defined by:

$$f_{band} = f_h / 2^s \quad (7)$$

Where f_h is the highest frequency component of the signal to be analyzed. Since the bandwidth of the harmonic wavelet is $2(n-m)\pi$, selection of the values for *m* and *n* of the HWPT has to satisfy the following conditions:

$$2(n-m)\pi = 2\pi f_{band} \tag{8}$$

Thus the harmonic wavelet packet coefficients *hwpt*(*s*, *i*, *k*) can be obtained as:

$$hwpt(s,i,k) = hwt(m,n,k) \tag{9}$$

Where *s* is the decomposition level, *i* is the index of the sub-band, *k* is index of the coefficient. The parameters *m* and *n* need to satisfy the following condition:

$$\begin{cases} m = i \times f_{band} = i \times \dfrac{f_h}{2^s} \\ n = (i+1) \times f_{band} = (i+1) \times \dfrac{f_h}{2^s} \end{cases} \quad i = 0,1,\cdots,2^s - 1 \tag{10}$$

2.3. AE Signal Feature Extraction

With the AE signal being decomposed into a number of sub-bands, the features can be extracted from the harmonic wavelet packet coefficients in each sub-band to provide information on the type of AE source. The fact of different energy distribution of signals in different frequency bands must be caused by the difference information contained in the signals. For the AE signal, because of the different AE source features, the characteristic energy distribution coefficient of harmonic wavelet packet is selected as the features. The energy content of a signal can be calculated, based on the coefficients of the signal's transform. In the case of a HWPT, the coefficients *hwpt*(*s*, *i*, *k*) quantify the energy associated with each specific sub-band. The details of feature extraction procedure are shown as follows.

Step 1: Normalizing the AE signal using:

$$\widetilde{\mathbf{X}} = D_\sigma^{-1}[\mathbf{X} - E(\mathbf{X})] \tag{11}$$

Where $\mathbf{X}$ is the AE signal, $E(\mathbf{X})$ and D_σ is the mean and standard deviation of $\mathbf{X}$.

Step 2: Decomposing $\widetilde{\mathbf{X}}$ with four levels of harmonic wavelet packet transform, and getting the coefficients vectors of the sixteen nodes, $H_{4,0}, H_{4,1}, \cdots, H_{4,15}$, where $H_{4,i}$ represents $hwpt(4,i,k)\ k = 0,1,\cdots N-1$, in which *N* is the length of AE signal.

Step 3: Calculating the energy of each node and normalizing them.

$$EH_{4,i} = \int \left|H_{4,i}\right|^2 dt = \sum_{j=1}^{N} \left|H_{4,i,j}\right|^2 \tag{12}$$

$$\overline{EH_{4,i}} = \frac{EH_{4,i}}{\sqrt{\sum_{i=0}^{15} |\, EH_{4,i}\,|^2}} \tag{13}$$

Step 4: the feature vector $T = [\overline{EH_{4,0}}, \overline{EH_{4,1}}, \overline{EH_{4,2}}, \cdots, \overline{EH_{4,15}}]$ is used to identify the AE source types.

3. AE Source Identification Using Hierarchy Support Vector Machine (H-SVM) Classifier

AE source identification is a typical problem of pattern recognition with small sample, because in most cases, it is difficult to obtain large sample sets of AE signals in composite material to train the classifiers. In this paper, support vector machine (SVM) is selected as the basic classifier, because it provides a novel approach to the two-category classification problem with good small sample generation [16-17].

The concept of composite damage was proposed by Professor K. L. Reifsnider [18] at 1977 during his research on composite fatigue damage. There are four damage types of fiber

composite, i.e. matrix cracking, interfacial debonding, delamination and fiber fracture. The task of AE source identification is to distinguish the damage type using the AE signals. Because the features of AE signal for interfacial debonding and delamination are similar and these two damage types are always occurred at the same time for the carbon fiber materials, in this paper, three damage types are studied, i.e. matrix cracking, interfacial debonding and fiber fracture. Obviously, AE source identification is a multi-classification problem.

There are two standard approaches to construct and combine the results from binary classifiers for a *C*-class problem. The first one is the one-vs-rest method, in which each classifier distinguishes one class from the other *C*-1 classes, and the class label of the input is decided by winner-take-all method [19]. Each classifier needs to be trained on the whole training set, and there is no guarantee that good discrimination exists between one class and the remaining classes. The second standard approach to combine binary classifiers is the one-vs-one method, in which the decision is made by majority voting strategies. This requires training and testing of *C*(*C*-1)/2 binary classifiers. This approach is prohibitive when *C* is large [20].

Thus, we chose a binary hierarchical classification structure in Figure 2. Each node is a binary classifier. Coarse separation among classes occurs in the beginning (at upper levels) in the hierarchy and a finer classification result is obtained in later (at lower levels). At the top node, we divide the original 4 classes into two smaller groups of classes (macro-classes). This clustering procedure is repeated in subsequent levels, until there is only one class in the final sub-group. This hierarchical structure decomposes the problem into 3 binary sub-problems. For testing, only about $\log_2 3$ classifiers are required to traverse a path from top to bottom.

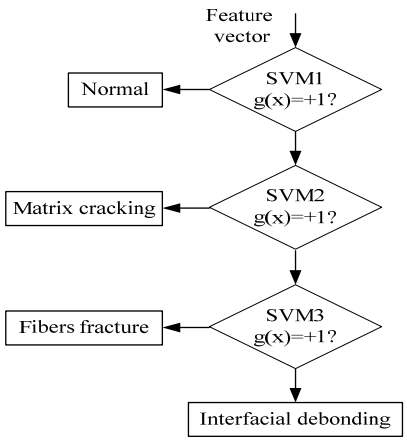

Figure 2. Hierarchical Multi-classification Structure for AE Source Identification

In this paper, the standard *k*-means clustering is used to design the binary hierarchical structure, as shown in Figure 2. SVM1 is used to classify Normal vs other three patterns, SVM2 is used to classify Matrix cracking vs Fibers fracture, Interfacial debonding, SVM3 is used to classify Fibers fracture vs Interfacial debonding.

In the training phase, the training samples are grouped according to Figure 2. Then SVM1 to SVM3 are trained using the corresponding group of training samples. After that, by inputting the feature vector into the trained multi-classifier, the AE source type can be identified.

4. Experiment and Results

4.1. Experimental Setup

In order to verify the proposed method, a series of pressure off experiments were carried out on the specimen of carbon fiber materials, which is one of the commonly used materials of helicopter moving component. The AE signal measurement system is shown schematically in Figure 3. Figure 4 shows the pressure off experiment process on carbon fiber specimen. The dimensions of all samples are all 418mm×120mm×2mm. Two AE sensors are distributed on the carbon fiber specimen, one is 80mm distance away from the central line of the

specimen in up direction, and the other is 80mm distance away from the central line of the specimen in down direction. The central point of the specimen is the force point. The loading speed of the pressure off experiment is 500N/s. Figure 5 is the AE signal acquisition system employed on-site. The signal conditioning is performed by the pre-amplifiers. The conditioned signal (with a gain of 40dB) is fed to the main data-acquisition board in which the AE waveforms and parameters are stored. The instruments and equipments used in the experiments are listed below:

(1) MTS electro-hydraulic loading system (MTS 810 material test system).
(2) Vallen AMSY-5 AE signal acquisition system with 16 channel and 16-bit, 10-MHz AD converter on each channel.
(3) Two Vallen VS150-M AE sensors.
(4) Two Vallen AEP4 pre-amplifiers (20-2000KHz).
(5) Vallen AE application software Vallen Visual AE.
(6) Notebook computer.

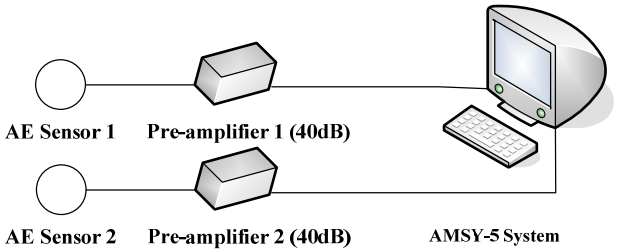

Figure 3. Schematic of the AE Measurement System

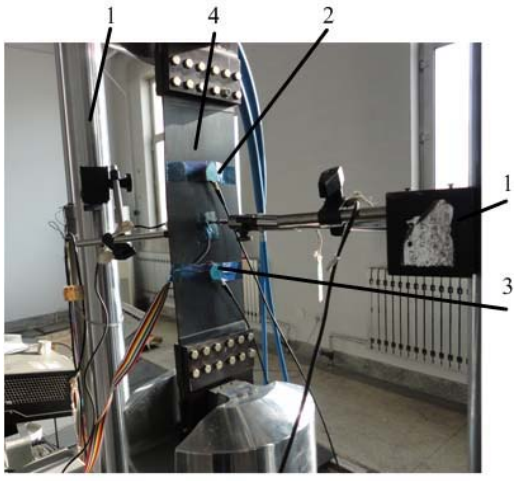

1. MTS electro-hydraulic loading system
2.AE sensor 1 3. AE sensor 2
4. Carbon fiber specimen

Figure 4. Pressure Off Experiment Process on Carbon Fiber Specimen

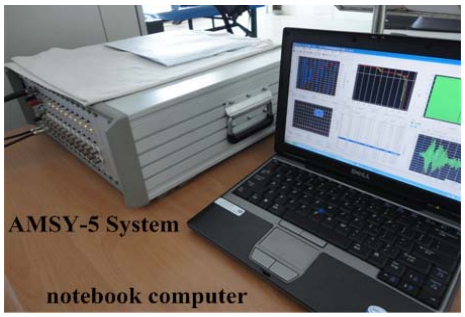

Figure 5. AE Signal Acquisition System Employed On-site

The sampling rate of the acquisition system is 1MHz. In order to acquire all AE signals during the pressure off process, AMSY-5 works in continuous acquisition mode. Three specimens of carbon fiber materials with the same dimensions are under the pressure off experiment. For each AE source type, 50 groups of data are gathered.

Figure 6, Figure 7 and Figure 8 shows the AE signal and its spectrum of matrix cracking, the AE signal and its spectrum of interfacial debonding and the AE signal and its

spectrum of fiber fracture, respectively. The three AE signal are all normalized using Equation (11). The spectrum of AE signal for the three types indicates that the energy distribution of the three types is different. The energy of matrix cracking is mainly in low frequency band and the frequency band is very narrow. The energy of interfacial debonding distributes in wide frequency band. The frequency band of fiber fracture is wider than matrix cracking but narrower than interfacial debonding.

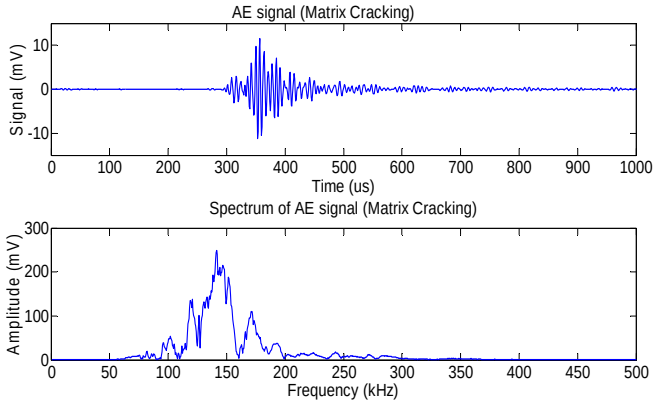

Figure 6. AE Signal and Its Spectrum of Matrix Cracking

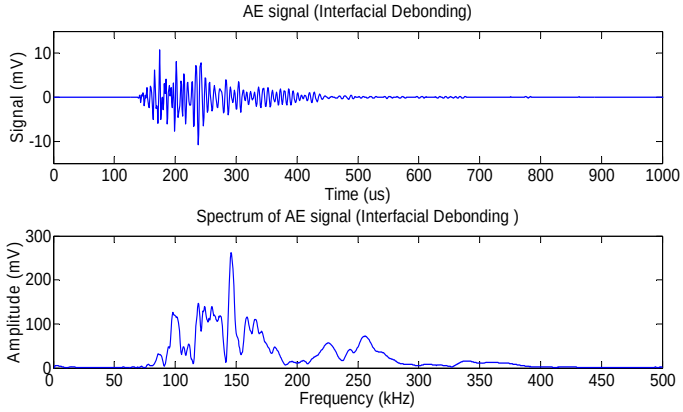

Figure 7. AE Signal and Its Spectrum of Interfacial Debonding

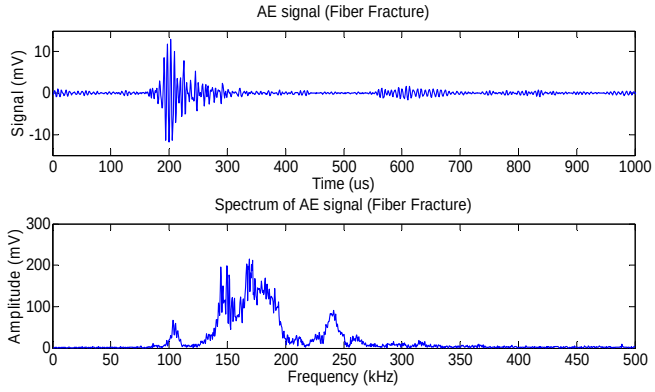

Figure 8. AE Signal and Its Spectrum of Fiber Fracture

AE source identification is a typical problem of pattern recognition with small sample, because in most cases, it is difficult to obtain large sample sets of AE signals in composite material to train the classifiers. In this paper, support vector machine (SVM) is selected as the basic classifier, because it provides a novel approach to the two-category classification problem with good small sample generation [16-17].

4.2. Feature Extraction

Firstly the experiment of feature extraction is performed according to the algorithm given in the section 1.3. Table 1 shows the feature nodes and their frequency ranges. The frequency band for each feature node is 31.25KHz. Figure 9 shows the normalized energy distribution for different AE sources at 15 frequency sub-bands.

Table 1. Feature Nodes and Their Frequency Band Range

Feature nodes	Frequency band No	Frequency band range (KHz)
H4,0	0	0~31.25
H4,1	1	31.25~62.5
H4,2	2	62.5~93.75
H4,13	13	40.625~43.75
H4,14	14	43.75~468.75
H4,15	15	468.75~500.00

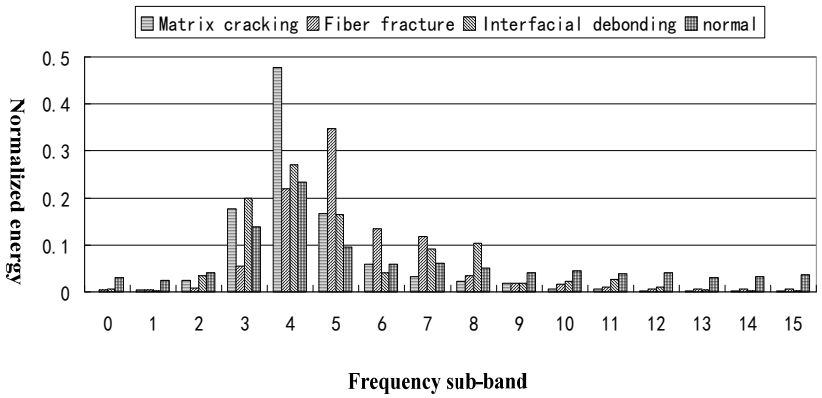

Figure 9. Normalized Energy Distribution for Different AE Source at 15 Frequency Sub-bands

As shown in Figure 9, the energy distribution of normal state is approximately uniform in every frequency band, because the AE signal of normal state is approximately white noise. The energy distribution of Matrix cracking is mainly concentrated in frequency band 3, 4 and 5. The energy distribution of Fibers breaking is mainly concentrated in frequency band 4, 5, 6, and 7. The energy distribution of interface separation is broad, approximately from frequency band 3 to 8. Therefore combining above analysis, the AE source types can be distinguished using the harmonic wavelet packet energy features.

4.3. AE Source Identification Using H-SVM Classifier

After the experiment of feature extraction, two groups of data are acquired, i.e. the training samples and the testing data. 20 groups of data for each type are used as training samples, and the other 30 groups of data for each type are used as testing data. The H-SVM classifier is trained using the training samples according to section 2. The kernel functions of the three SVMs in the H-SVM classifier are all selected as RBF kernels, shown as Equation (14). The kernel width parameter, σ , for each SVM is selected as 1.0.

$$K(X_i, X_j) = \exp(-\left\|X_i - X_j\right\|^2 / \sigma^2) \quad (14)$$

Table 2 shows the AE source identification result using HWPT and H-SVM. The results indicate that the proposed approach can implement AE source type identification effectively

Table 2. AE Source Identification Result Using HWPT and H-SVM

AE source type	Test sample No (Correct No)	Identification rate (%)
Matrix cracking	30 (28)	93.33
Fibers breaking	30 (27)	90.00
Interface separation	30 (28)	93.33
Normal	30 (30)	100.00

In order to verify the advantages of the HWPT feature extraction, the comparison of WPT feature extraction and H-SVM classifier with HWPT and H-SVM is studied. For the WPT feature extraction, the wavelet function is selected as Db10, and the decomposing level is also 4. Similar to the HWPT feature extraction, the feature vector of WPT is also the normalized energy in each frequency band. Table 3 shows the comparison of feature extraction time for HWPT and WPT. These algorithms are all implemented by Matlab 7.1 on Intel Dual Core 2.4GHz and 1G RAM. The results indicate that the feature extraction speed of HWPT is over nine times as quick as the WPT. Such an advantage of the HWPT over WPT is even more appreciable when the decomposition level is larger than 4, because of the additional recursive operations needed for WPT.

Table 3. Feature Extraction Time Comparison of HWPT and WPT

Feature extraction method	Feature extraction time for 50 samples (s)
HWPT	0.65
WPT	5.88

Table 4 shows the comparison of AE source identification result for HWPT and H-SVM with WPT and H-SVM. The results indicate that the identification rate of HWPT and H-SVM is a little higher than WPT and H-SVM. HWPT overcomes the energy leakage shortcoming of traditional wavelet, and can extract the energy feature more accuracy.

Table 4. AE Source Identification Comparison of HWPT and H-SVM with WPT and H-SVM

AE source type	Identification rate (%)	
	HWPT and H-SVM	WPT and H-SVM
Matrix cracking	93.33	86.67
Fibers breaking	90.00	83.33
Interface separation	93.33	90.00
Normal	100.00	100.00

In order to verify the advantages of the H-SVM classification, the comparison of HWPT feature extraction and H-SVM classifier with HWPT and RBF neural network is studied. The RBF neural network is a three layer network. The first layer is the input layer, and the second layer has RADBAS neurons as well as the output layer has PURELIN neurons. For the classification of AE source type, the input neurons are 16, each for one feature. The output neurons are 4. Figure 10 shows the structure of RBF neural network for AE source classification. Table 5 shows the relationship between RBF output and AE source type.

Table 5. Relationship between RBF Output and AE Source Type

AE source type	Output of RB neural network [Y_1 Y_2 Y_3 Y_4]
Matrix cracking	[1 0 0 0]
Fibers breaking	[0 1 0 0]
Interface separation	[0 0 1 0]
Normal	[0 0 0 1]

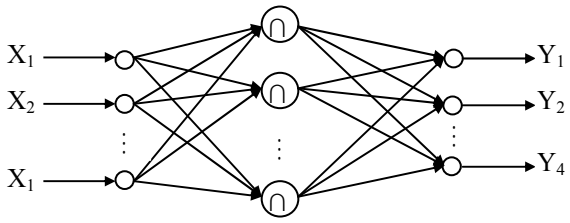

Figure 10. Structure of RBF Neural Network for AE Source Classification

The training process of the RBF neural network is shown as follows. Initially the RADBAS layer has no neurons, while the input layer has 16 neurons and the output layer has 4 neurons. The following steps are repeated until the network's mean squared error falls below GOAL or the maximum number of neurons are reached:

(1) The network is simulated using the training samples.
(2) The input vector with the greatest error is found.
(3) A RADBAS neuron is added with weights equal to that vector.
(4) The PURELIN layer weights are redesigned to minimize error.

Table 6 shows the comparison of training time for H-SVM and RBF neural network. These algorithms are all implemented by Matlab 7.1 on Intel Dual Core 2.4GHz and 1G RAM. The results indicate that the training speed of H-SVM is about three times as quick as the RBF neural network, which verify that the convergence performance of SVM is better than RBF neural network.

Table 6. Training Time Comparison of H-SVM and RBF Neural Network

Classification method	Training time for 20 samples (s)
H-SVM	0.120
RBF neural network	0.358

Table 7 shows the comparison of AE source identification result for HWPT and H-SVM with HWPT and RBF neural network. The results indicate that the identification rate of HWPT and H-SVM is higher than HWPT and RBF neural network, which verify that SVM is very suitable for classification with small training samples.

Table 7. AE Source Identification Comparison of HWPT and H-SVM with HWPT and RBF Neural Network

AE source type	Identification rate (%)	
	HWPT and H-SVM	WPT and RBF neural network
Matrix cracking	93.33	83.33
Fibers breaking	90.00	80.00
Interface separation	93.33	66.67
Normal	100.00	90.00

5. Conclusion

In this paper, the HWPT feature extraction and H-SVM classifier are firstly applied to the AE source identification. The experimental system is built up and the pressure off experiments on specimen of carbon fiber materials is carried out. The comparison results of HWPT and H-SVM with WPT and H-SVM indicate that the proposed approach can implement AE source type identification effectively, and it has better performance on computational efficiency and identification accuracy than WPT feature extraction. The comparison results of HWPT and H-SVM with HWPT and RBF neural network indicate that the proposed approach has better performance on computational efficiency and identification accuracy than the RBF neural network classification. The proposed approach is very suitable for small samples

problem. The efficient energy feature extraction ability and less computational time makes the HWPT and H-SVM good candidates for efficient, on-line AE source identification.

Acknowledgements

The authors would like to thank the financial support of the Natural Science Foundation of Liaoning 2013024010, and the financial support of the National Natural Science Foundation of China NSFC-61104023.

References

[1] Tittmann BR, Yen CE. Acoustic emission technique for monitoring the pyrolysis of composites for process control. *Ultrasonics.* 2008; 48(6-7): 621-630.
[2] Liu Q, Chen X. Fuzzy pattern recognition of AE signals for grinding burn. *Machine Tools & Manufacture*. 2005; 45(7-8): 811-818.
[3] Wang XH, Zhu CM, Mao HL, Huang ZF. Wavelet packet analysis for the propagation of acoustic emission signals across turbine runners. *NDT&E International.* 2009; 42(1): 42-46.
[4] Zhou R, Bao W, Li N, Huang X, Daren Yu. Mechanical equipment fault diagnosis based on redundant second generation wavelet packet transform. *Digital Signal Processing.* 2010; 20(1): 276-288.
[5] Feng ZG, Wang Q, Katsunori S. Design and implementation of a self-validating pressure sensor. *IEEE Sensors Journal.* 2009; 9(3): 207-218.
[6] Nikolaou NG, Antoniadis IA. Rolling element bearing fault diagnosis using wavelet packets. *NDT&E International.* 2002; 35(3): 197-205.
[7] Zhang WB, Zhou XJ, Lin Y. Harmonic wavelet package method used to extract fault signal of a rotation machinery. *Journal of Vibration and Shock*. 2009; 28(3): 87-89.
[8] Yan RQ, Robert X. An efficient approach to machine health diagnosis based on harmonic wavelet packet transform. *Robotics and Computer-Integrated Manufacturing*. 2005; 21(4-5): 291-301.
[9] Zhao YX, Xu YG, Gao LX. Fault pattern recognition technique for roller bearing acoustic emission based on harmonic wavelet packet and BP neural network. *Journal of Vibration and Shock.* 2010; 29(10): 162-165,257.
[10] Emamian V, Kaveh M, Ahmed H. Robust Clustering of Acoustic Emission Signals Using Neural Networks and Signal Subspace Projections. *EURASIP Journal on Applied Signal Processing*. 2003; 2003(3): 276-286.
[11] Kim KB, Yoon DJ, Jeong JC, Lee SS. Determining the stress intensity factor of a material with an artificial neural network from acoustic emission measurements. *NDT&E International*. 2004; 37(6): 423-429.
[12] Huguet S, Godin N, Gaertner R, Salmon L, Villard D. Use of acoustic emission to identify damage modes in glass fibre reinforced polyester. *Composites Science and Technology*. 2002; 62(10-11): 1433-1444.
[13] Newland DE. *Harmonic wavelet analysis.* Proc. R. Soc. Land, A. 1993; 443: 203-225.
[14] Newland DE. Harmonic wavelet analysis. *Part 1: Theory, Trans. ASME J. Vibration &Acoustic.* 1994; 116: 409-416.
[15] Newland DE. Harmonic wavelet analysis. *Part 2: Wavelet map, Trans. ASME J. Vibration &Acoustic.* 1994; 116: 417-425.
[16] Qian HM, Mao YB, Xiang WB, Wang ZQ. Recognition of human activities using SVM multi-class classifier. *Pattern Recognition Letters.* 2010;, 31(2): 100-111.
[17] Derya A, Asaf V. An expert diagnosis system for classification of human parasite eggs based on multi-class SVM. *Expert Systems with Applications*. 2009; 36(1): 43-48.
[18] Reifsnider KL, Lauraitis KN. Fatigue of filamentary composite materials. *ASTM Standards and Engineering Digital Library*. 1977: 100-112.
[19] Anand JR, Mehrotra K, Mohan CK, Ranka S. Efficient classification for multiclass problems using modular neural networks. *IEEE Transactions on Neural Networks.* 1995; 6(1): 117-124.
[20] Kumar S, Ghosh J, Crawford MM. Hierarchical fusion of multiple classifiers for hyperspectral data analysis. *Pattern Analysis and Applications*. 2002; 5(2): 210-220.